Lab on a Chip

PAPER

Check for updates

Selective cell encapsulation, lysis, pico-injection and size-controlled droplet generation using traveling surface acoustic waves in a microfluidic device†

Kirk Mutafopulos, [ab] Peter J. Lu, [ac] Ryan Garry,[a] Pascal Spink [ab] and David A. Weitz [*ac]

We generate droplets in a microfluidic device using a traveling surface acoustic wave (TSAW), and control droplet size by adjusting TSAW power and duration. We combine droplet production and fluorescence detection to selectively-encapsulate cells and beads; with this active method, the overwhelming majority of single particles or cells are encapsulated individually into droplets, contrasting the Poisson distribution of encapsulation number that governs traditional, passive microfluidic encapsulation. In addition, we lyse cells before selective encapsulation, and pico-inject new materials into existing droplets.

1 Introduction

Generating micron-scale droplets within a microfluidic channel enables many applications, including the encapsulation of cells or reagents in pico- or femto-liter volumes and screening single-cell assays at the single molecule level.[1–4] In most cases, passive methods have been used to form these droplets, wherein a population of cells or particles suspended in an aqueous solution (the dispersed phase) is flowed into an immiscible fluid, typically non-aqueous (the continuous phase), so that the reagents, cells, and reaction products are contained within a controlled micro-environment or pico-liter-scale reaction-flask.[5–8] These passive methods provide a simple, high-throughput way to produce droplets, requiring neither complex external apparatus nor active elements within the microfluidic device, and underlie such methods as the co-encapsulation of single cells with lysis buffers to perform directed enzyme evolution, and single-cell barcoding.[9–11] However, passive methods of droplet production suffer a fundamental limitation: they cannot control directly the number of cells encapsulated in each droplet; instead, this number is dictated by physics to follow a Poisson distribution, constraining the fraction of droplets that contain any specific number of cells. As a result,

all passive encapsulation devices face a trade-off between either a high fraction of empty droplets, or a higher fraction of droplets with multiple cells or particles; neither of these is typically desired, and this trade-off limits the effective rate at which single cells can be encapsulated.[7–13] Furthermore, passive devices lack the ability to select which cells to encapsulate, require additional aqueous channels for the inclusion of lysis reagents to break open cell membranes for single cell sequencing,[11,14] and are unable to incorporate additional reagents to already-formed droplets selectively in cases where multi-step reactions are required.[15] When specific sub-populations of cells need to be isolated from a heterogeneous population after encapsulation, the user often performs additional steps after passive encapsulation, such as sorting droplets that contain either particular materials, or a specific number of cells or particles per droplet; these added steps usually require additional microfluidic devices, which increase complexity and decrease final yields.[16,17] A single device that could produce and manipulate droplets and their contents actively has the potential to obviate many additional steps, and could be extremely advantageous to many droplet-based microfluidic procedures and protocols.

Several active droplet-generation methods have been developed to overcome the limitations of passive droplet production, such as pulsed lasers,[18] *trans*-interface electric-potential generation,[19] integrated micro-pumps,[20] and travelling surface acoustic waves (TSAW).[21] Poisson statistics do not apply to the encapsulation using these active methods, which require fewer downstream steps to improve the distribution of occupied droplets. Among these methods, generating SAWs with an interdigital transducer (IDT) allows

a School of Engineering and Applied Sciences, Harvard University, Cambridge, MA, 02138, USA. E-mail: weitz@seas.harvard.edu
b Cytonome/ST, LLC, Bedford, MA, 01730, USA
c Department of Physics, Harvard University, Cambridge, MA, 02138, USA

active manipulation of both fluids and particles simultaneously on microsecond timescales, and is therefore an excellent candidate for integrating on-demand droplet generation,[21,22] encapsulation, cell lysis,[23] and pico-injection onto a single microfluidic device.[21,24] Furthermore, IDT-based TSAW microfluidics have been readily integrated with fluorescence-activated control techniques, such as fluorescence-activated cell sorting (FACS).[25–29] Consolidating these techniques in a single device—for instance to select cells and encapsulate them in droplets, or to control the addition of reagents to existing droplets for multi-step reactions—would increase the efficiency and performance of a broad range of microfluidics-based investigations.

In this work, we present a microfluidic device methodology that combines fluorescence detection, an IDT to generate travelling surface acoustic waves (TSAW), and step-emulsification channel geometries to produce on-demand droplets with controllable size. We actively encapsulate cells and beads into micron-sized droplets in response to fluorescence detection; the resulting distribution of droplet occupancy is dominated by droplets containing only one single cell, which has never been achieved using passive encapsulation methods. We increase the power and duration of the TSAW pulse to lyse and encapsulate cells in a single step. Finally, we controllably pico-inject fluid into existing droplets. Together, these techniques, which can be integrated on a single device, open up a large range of new droplet microfluidics applications.

2 Results and discussion

2.1 Device design

Our device incorporates channels molded from polydimethylsiloxane (PDMS), with two inlets and two outlets; these form two separate parallel fluidic channels of width $\Delta y = 70$ μm but with different heights, which come into contact only within a small channel-contact region of length $\Delta x = 45$ μm, as shown in the $\hat{x}$–$\hat{y}$ device schematic in Fig. 1a. We plasma-bond the PDMS to a piezoelectric lithium niobate (LiNbO$_3$) crystal substrate patterned with the tapered gold IDT that generates the TSAW. Our tapered IDT design facilitates precise positioning of the generated TSAW[25,28–30] along the $\hat{x}$-direction by varying its resonant frequency, thereby allowing precise control of the TSAW propagation path within the channel-contact region where the dispersed and continuous phases come into contact, as shown in Fig. 1b–d. We flow an aqueous dispersed phase (1XS PBS) into the channel of height $\Delta z = 30$ μm adjacent to the IDT at 0.5 mL h^{-1}, and a non-aqueous continuous phase (HFE-7500, 3M) into the taller channel of height $\Delta z = 60$ μm on the side opposite from the IDT at 5 mL h^{-1}. We use a spiral channel for the aqueous phase to spatially order cells and beads into a straight line via inertial flow focusing, as shown in Fig. 1a.[29] We place the IDT in an air gap separated from the fluidic channels by a PDMS wall of width $\Delta y = 50$ μm, as shown in the $\hat{y}$–$\hat{z}$ cross section of the channel contact region in Fig. 1b–d.
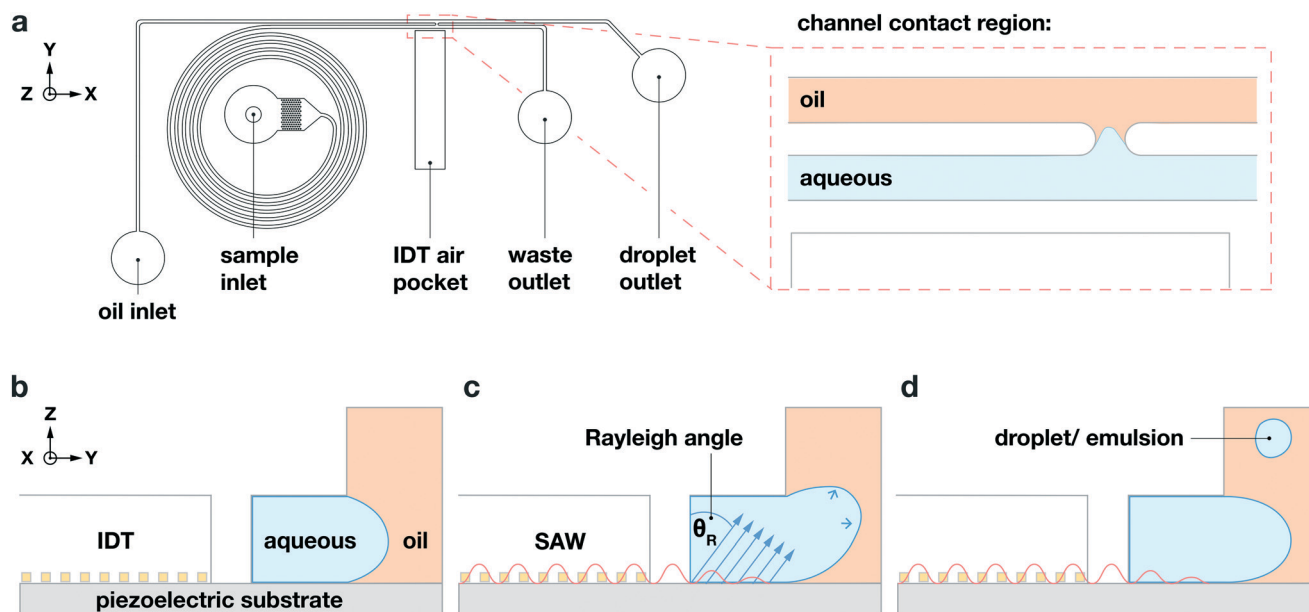

Fig. 1 Droplet generation using TSAW in a microfluidic device. (a) General schematic of the microfluidic device and the contact region between the aqueous (blue) and non-aqueous oil (orange) channels, adjacent to the air pocket through which the TSAW propagates. (b)–(d) Droplet generation. Flow direction is in the $\hat{x}$-direction, towards the reader. (b) When the IDT is not actuated, no droplets are generated and no aqueous liquid flows into the adjoining non-aqueous oil channel. (c) When the IDT is actuated, it generates a TSAW that propagates into the aqueous fluid on the near side of the channel; this leaky TSAW displaces the aqueous liquid along a vector whose direction relative to the vertical $\hat{z}$-axis is governed by the Rayleigh angle, which in the present coordinate system is positive in both $\hat{y}$ and $\hat{z}$ directions, thereby pushing the aqueous phase into the taller non-aqueous channel. (d) Once in the taller non-aqueous channel, the aqueous phase pinches off due to the gradient in the Laplace pressure between the two fluids, generating a droplet of aqueous phase surrounded by non-aqueous oil phase.

2.2 On-demand droplet generation

When the IDT-generated TSAW propagates from this air gap through the PDMS and into the liquid-filled channel, it creates a longitudinal wave in the liquid at the Rayleigh angle (θ_R) that attenuates within a few micrometers and displaces aqueous fluid[31,32] in the contact region into the non-aqueous phase; the abrupt change in channel height facilitates the pressure drop that induces the pinch-off of the dispersed phase, forming single droplets *via* step-emulsification, as illustrated in Fig. 1b.[33–36] By contrast, similar devices with a single channel height, and therefore no step, produce virtually no droplets (Video S1†). Critically, we generate droplets on-demand, only when we activate the IDT; otherwise, we do not observe the spontaneous formation of droplets. Qualitatively, increasing either the power level or pulse length pushes more fluid from the aqueous channel into the non-aqueous channel, increasing the size of the resulting droplets, as shown in Fig. 2. To quantify the effects of these factors on size, we actuate the IDT at different power levels and different pulse lengths, and measure the size of the resulting droplets produced; we find that the droplet size increases roughly linearly as a function of power and duration increases, as shown in Fig. 3.

2.3 Selective encapsulation

Standard encapsulation of cells or beads into droplets in commonly-used passive devices without active elements leads to a distribution of droplet occupancy that is described by the Poisson distribution—which leaves most droplets empty. These passive techniques do not allow increasing the fraction of droplets that encapsulate only a single object without concomitantly increasing the fraction encapsulating multiple objects, which is typically undesired. By contrast, active
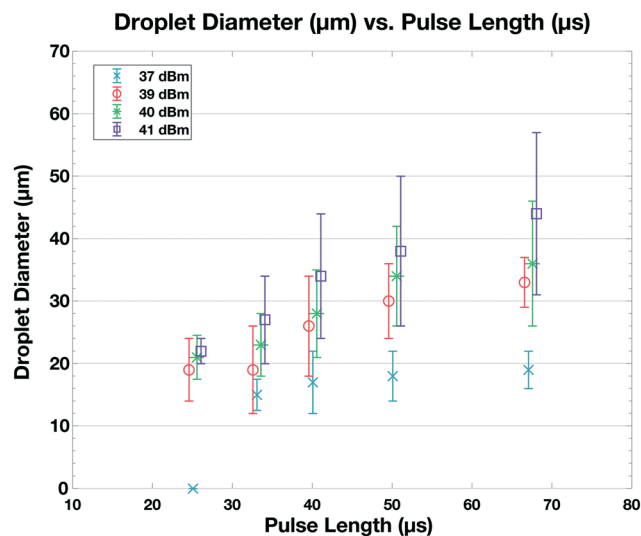

Fig. 2 TSAW-activated droplet production. Individual frames exported from a high-speed camera. (a)–(c) IDT set to 41 dBm and a 40 μs pulse length, which produces a droplet approximately 38 μm in diameter. (d)–(f) IDT set to 37 dBm and a 33 μs pulse length, which produces a droplet approximately 17 μm in diameter.

Fig. 3 Droplet diameter (μm) as a function of pulse length (μs) and power level (dBm). As either the pulse length or power of the TSAW increases, the droplet diameter increases in an approximately linear manner.

methods, which encapsulate objects on demand, do not generate an occupancy distribution necessarily described by Poisson statistics; consequently, these devices can at least in principle generate a larger population of droplets where the majority contain only a single bead or cell, substantially increasing efficiency and possibly obviating downstream sorting and processing steps. We investigate this possibility with our TSAW apparatus in a manner analogous to microfluidics-based fluorescence-activated cell sorting (FACS), with a key difference that we do not simply displace particles or cells of interest into separate channels with aqueous solutions; instead, we combine fluorescence sorting with the on-demand droplet formation described above.

To test our methodology, we flow a mixture of 10 μm yellow-green fluorescently-labeled beads (Spherotech) with unlabeled K562 cells (15 μm) at a total concentration of 1×10^6/mL in an aqueous medium (1× PBS, 10% Opti-prep) at 0.5 mL h^{-1}. For the non-aqueous phase, we flow HFE-7500 at 5 mL per hour through the non-aqueous channel. We interrogate the beads and cells with a 488 nm laser (Toptica), and when the PMT detects a fluorescent signal, we activate the IDT; this displaces the bead and its surrounding fluid into the non-aqueous channel, pinching off a droplet which contains only that single bead, in a manner entirely analogous to that used to generate droplets. Using a power level of 39 dBm and pulse length setting of 50 μs, we successfully separate out fluorescent beads and immediately encapsulate them in droplets with an average diameter of 35 μm, as shown in Fig. 4a–d (Video S2†). We take images with a high-speed camera (Hi-Spec) and randomly sample fifty droplet-generation events, plotting the fraction of droplets that contain no beads, one bead, or more multiple beads, and compare this to a corresponding Poisson distribution; we find that the overwhelming majority of droplets from our
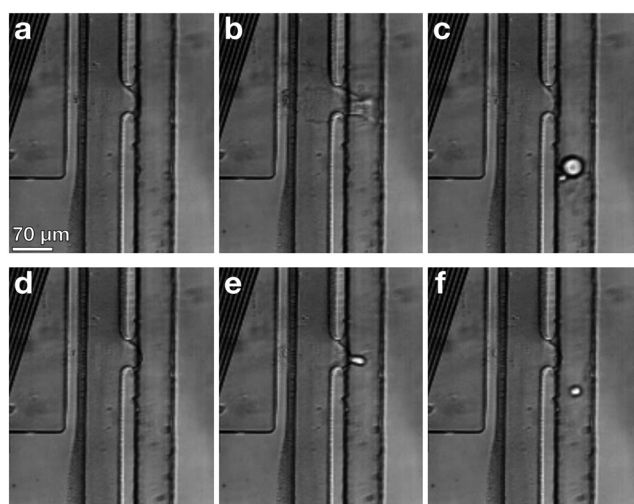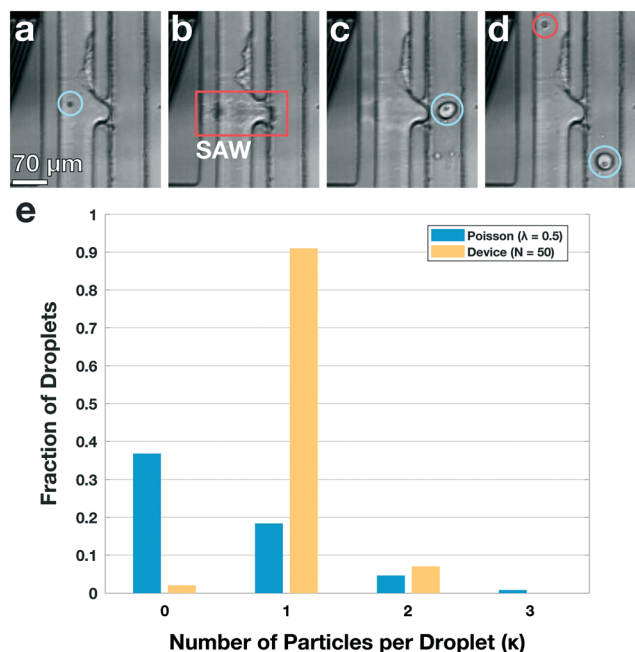
Fig. 4 Active, on-demand encapsulation using TSAW overcomes the Poisson-distribution limitation on droplet occupancy. (a)–(d) Individual frames exported from a high-speed video of a 10 μm bead being deflected and encapsulated upon detection. (a) Green fluorescent 10 μm bead (blue circle) flows past a 488 nm laser (not visible) and is detected. (b) The IDT is actuated and produces a TSAW into the channel to deflect and encapsulate the bead at the contact region (red box). (c) A droplet is created containing the detected bead (blue circle) and an incoming unlabeled K562 cell enters the outlet channel. (d) A droplet containing the bead (blue circle) flows out of the device through the non-aqueous channel and the K562 cell (red circle) continues to flow past the IDT and is not encapsulated (not shown, see Video S2†). (e) Fraction of droplets containing no beads, a single bead, or more than one bead. The overwhelming majority of droplets from the device have a single particle encapsulated (yellow bars); by contrast, the droplet occupancy of all passive devices is governed by a Poisson distribution, shown for a theoretical calculation using $\lambda = 0.5$ (blue bars). The Poisson case shows significant higher numbers of empty and multiply-occupied droplets, both of which are undesirable and may require subsequent sorting or filtering to mitigate.

device encapsulate a single bead, as shown in Fig. 4e, providing strong quantitative evidence that we able to overcome the limitations imposed by Poisson statistics.

2.4 Simultaneous cell lysis and encapsulation

Our device deflects and encapsulates live cells on-demand using a relatively gentle displacement, allowing the overwhelming majority of cells to remain alive and healthy. At the opposite limit, with a much stronger pulse from the IDT, we find that cells may be damaged. In some cases, where cell viability is desired, this is a drawback; in other cases, this can be a feature: lysing a single cell and then immediately capturing its contents in a single droplet would facilitate single-cell resolution for a host of techniques, including single-cell sequencing, transcriptomics, and

proteomics.[37–39] At present, these single-cell techniques, both in bulk and in droplets, rely on chemicals to break down the cell membrane or cell wall, lysing the cells and exposing their internal contents;[38,40–42] how these chemical lysing agents affect genetic and protein materials is not in general known,[38] and at least in principle, a purely mechanical way to lyse cells and encapsulate their contents could be desirable.

To test the ability of our device to lyse and encapsulate cells, we prepare a suspension of green-fluorescent calcein AM and red-fluorescent ethidium homodimer-1 (LIVE/DEAD Kit, Cat# L3224 Thermo Fisher) labeled and unlabeled K562 cells at a concentration of 10^6 cells per mL, and flow the suspension into the device at a flow rate of 0.5 mL h^{-1}; we set the flow rate of the continuous phase to 5 mL h^{-1}. We trigger the IDT based on fluorescence detected from calcein AM labeled cells excited by the laser at $\lambda = 488$ nm, and evaluate cell viability using the LIVE/DEAD kit by imaging cell-bearing droplets in a confocal microscope (Leica SP5). Using a power level of 41 dbm and pulse length of 67 μs, we successfully deflect and encapsulate cells individually into droplets, and the cells are unharmed, as shown in Fig. 5a–d. We then increase the power level to 43 dBm, holding other conditions fixed, and observe that the TSAW breaks the cell membrane and then immediately forces the creation of a droplet that encapsulates the cell contents, as shown in Fig. 5e–h.

2.5 Pico-injection

Our multi-channel chip design may also enable the integration of additional active on-chip procedures, such as
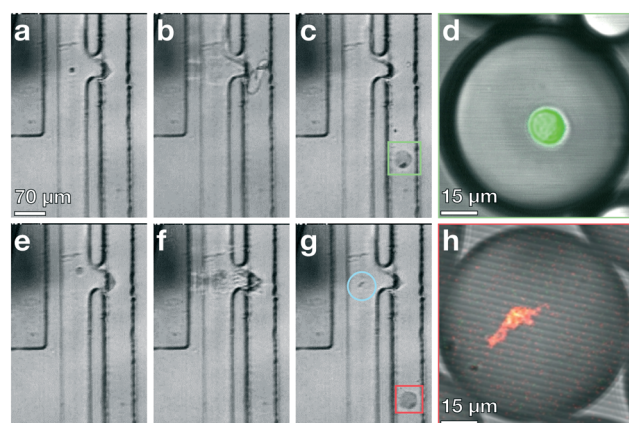

Fig. 5 Simultaneous cell encapsulation and lysis. (a)–(c) Individual frames exported from a high-speed camera of a fluorescent K562 cell encapsulated (green box) using a power level and pulse length of 41 dBm and 67 μs, respectively. (d) Image of an encapsulated cell taken with a confocal microscope, demonstrating successful encapsulation of the intact cell. (e)–(g) Individual frames exported from a high-speed camera of a K562 cell lysed and then encapsulated, using a power level and pulse length of 43 dBm and 67 μs, respectively. Residual cellular debris remains in the aqueous phase channel (blue circle), with a droplet containing the remaining cell components (red square). (h) Image of an encapsulated lysed cell taken with a confocal microscope.

the on-demand injection of reagents into existing droplets. Existing methods for such pico-injection typically flow surfactant-stabilized droplets past a channel containing the pressurized reagent to be added; an electric field is applied, which destabilizes the droplet surfactant layer, rupturing the film separating droplet and reagent, and facilitating coalescence.[15,43,44] To add fluid to existing droplets using the TSAW, we modify our previously-described device so that the channels are the same height of $\Delta z = 30$ μm, thereby removing the step; lengthen the channel-contact region to $\Delta x = 55$ μm; re-position the IDT so that it is directly opposite where the channels come into contact; and add a T-junction droplet maker to the non-aqueous channel,[4,45] as shown in the schematic in Fig. 6a. We flow the same aqueous (1× PBS, 0.5 mL h^{-1}) and non-aqueous (HFE-7500, 2 mL h^{-1}) fluids as above, in addition to using the aqueous phase to create the water-in-oil droplets with the T-junction (0.125 mL h^{-1}); to facilitate imaging, we add fluorescein to the aqueous channel. We set the flow rates in the aqueous, non-aqueous, and droplet-generation channels to 2, 0.5 and 0.125 mL h^{-1}, respectively, and observe with a fast camera that the droplet-maker generates droplets at 125 Hz. We synchronize manually the relative phase of the IDT that generates a TSAW with the same frequency as the droplet maker, and find that for pulses with power greater than 41.5 dBm and duration of 33 μs, the TSAW is sufficiently powerful to break the surface tension of a droplet that is present in the contact region, as shown in Fig. 6b–j. When the droplet is ruptured by the

TSAW, it coalesces with the dyed aqueous fluid at the contact region, enabling the fluorescein dye to flow into the droplet already in the non-aqueous channel, as shown in Fig. 6k (Video S3†).

We collect unaltered droplets from the outlet of the non-aqueous channel, when the IDT is not activated; and pico-injected droplets, using the IDT. We observe both sets of output droplets in a laser-scanning confocal microscope (Leica SP5) with $\lambda_{exc} = 488$ nm, in both transmission and fluorescence modes. We find that the unaltered droplets contain no significant dye, and are thus not visible with fluorescence but clearly visible in transmission, where we measure their diameter to be approximately 75 μm. By contrast, the pico-injected droplets are highly visible in fluorescence as well as in transmission, and we measure their diameter at 86 μm (additional volume is due to the pico-injection of the additional dyed aqueous fluid), as shown in Fig. 6k.

3 Materials and methods

3.1 Device design

The device consists of a PDMS sorting chip containing the device's flow channels bonded to a substrate beside an IDT. Drawings of the IDT design and the microfluidic device are created using AutoCAD (Autodesk; San Rafael, CA). Structures defined in the drawings are transferred to photomasks for lithography, which are used to fabricate molds for PDMS
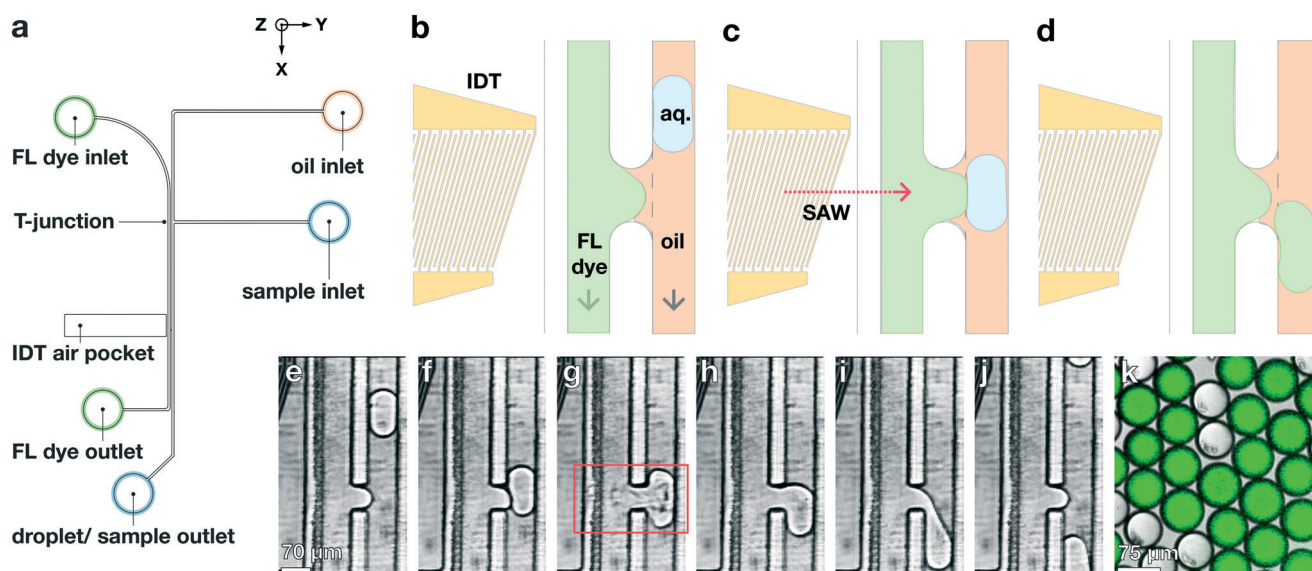

Fig. 6 Pico-injection with TSAW. (a) Device schematic. Green fluorescent dye is flowed through the FL dye inlet. 1× PBS (dispersed phase) and HFE-7500 (continuous phase) are flowed into the sample inlet and oil inlet, respectively. The dispersed phase is flowed into the continuous phase orthogonally, which produces droplets. These droplets flow down the channel in the $\hat{x}$-direction, past the channel contact region where a TSAW is generated to inject the green fluorescent dye into the droplets. (b)–(d) Schematic of pico-injection in the channel-contact region. When the droplet comes into contact with the green fluorescent dye, the IDT is triggered to produce a TSAW which breaks the surface tension and enables the aqueous phases of the two interfaces to coalesce, so that the dye enters the droplet. (e)–(j) Individual frames exported from a high-speed camera of a PBS in oil droplet injected with green florescent dye. As the droplet comes into contact with the dye, the TSAW is generated in the channel $\hat{y}$-direction, enabling the dye to enter the droplet (red box). When the TSAW is no longer generated, the droplet continues to flow in the $\hat{x}$-direction, pinching off from the fluorescent dye. (k) Confocal microscope image of droplets collected from the device, with and without green pico-injected fluorescent dye. When the IDT is powered off pico-injection does not occur.

replicas. The device uses an IDT with a tapered-finger design,[28–30] characterized by a continuously-changing pitch of the IDT fingers from one side to the other, effectively varying the resulting position laterally along the transducer of a TSAW at a given resonant frequency, which ranges from 155 to 179 MHz. The width of the excited TSAW beam can be approximated by the electrode aperture and the frequency difference between each IDT pole,[30] and is approximately 30 μm in our design. The metallization ratio a/p, the fraction of the electrode width a and pitch p, is 0.5 throughout the transducer. Electrodes on either pole are interconnected by trapezoidal bus bars that merge into square contact pads to apply external voltages. The trapezoidal bus shape prevents the IDT from obstructing the flow channels of the PDMS slab.

The microfluidic device contains two layers, each fabricated using a separate photomask. The first layer contains the aqueous (dispersed phase) channel and the air pocket for the IDT. The second layer contains the oil (continuous phase) channel. The sample inlet consists of a 70 μm-wide spiral channel that leads to the droplet-generation region. The air pocket is a rectangular-shaped area that prevents acoustic waves from leaking into the PDMS device away from the intended droplet-generation region. The thickness of the PDMS separating the air pocket from the liquid in the sorting region is minimized to 50 μm to reduce power loss while maintaining fluidic sealing. Each layer contains two sets of alignment marks consisting of an asymmetrical pattern of crosses, enabling the two layers to be aligned precisely. The masks for the individual layers (CAD/Art Services; Bandon, OR) are imaged with a resolution of 15 400 dpi.

3.2 IDT fabrication

The IDTs are fabricated in a lift-off process using a modified protocol from the Center for Nanoscale Systems at Harvard University. For the piezoelectric substrate, we use 4 inch diameter black 128° *Y–X* cut lithium niobate double-side polished wafers that are 500 μm thick; these offer adequate optical transparency, strong electro-mechanical coupling with low bulk wave generation, and high TSAW velocity.[30] In addition, the black, chemically-reduced lithium niobate helps facilitate fabrication steps that involve baking on heat plates by effectively eliminating the pyroelectric effect.[46] Each wafer is cleaned with acetone and isopropanol. Any residual moisture on the wafer is removed with a dehydration bake on a heat plate at 180 °C for at least 3 minutes. For every step involving baking, the wafer is held 5 to 10 mm above the heat plate surface for about 20 seconds before placing it down, to ease temperature changes of the substrate and reduce the risk of cracking. Consequently, hot wafers are held in air for about 20–30 seconds to gently cool down the substrate to room temperature before proceeding with any next steps. A 300 nm sacrificial layer is created by spin-coating LOR 3A (MicroChem; Westborough, MA) at 3000 rpm on the cleaned

wafer surface, followed by baking the layer at 180 °C for 7 minutes. Subsequently, Shipley S1805 (MicroChem) is spun at 4000 rpm to form a 500 nm layer of photoresist on top of the sacrificial layer and baked for 1 minute at 115 °C. The coated wafers are exposed to a UV dosage of 40 mJ cm^{-2} and a wavelength of 405 nm using a mask-less alignment tool (MLA150, Heidelberg Instruments; Heidelberg, Germany) to transfer the designed IDT patterns to the substrate. The exposed patterns are developed in CD-26 developer (Microposit MF; Dow Electronic Materials, Marlborough, MA) during a 75 second-long immersion, followed by a rinse with deionized water and drying the wafer with nitrogen.

Prior to metal deposition, wafers are cleaned with oxygen plasma for 5 minutes at 150 W and 40 sccm gas flow (Anatech SCE-106 plasma barrel etcher, Anatech USA; Union City, CA) to remove organic residues from the substrate surface that could impair metal adhesion. Electron beam physical vapor deposition (Denton Explorer 14, Denton Vacuum; Moorestown, NJ) is used to create a 10 nm thick titanium adhesion layer, followed by 50 nm of gold to form IDTs on the wafer. To obtain the IDTs, the deposited wafers are soaked in a Remover-PG bath (MicroChem) at 80 °C for about 3 hours to lift-off the sacrificial layer and cleaned with isopropanol. To facilitate plasma bonding between the PDMS molded channels and the piezoelectric substrate, the wafers containing the IDTs are covered with a 50 nm thick layer of SiO_2 in a sputtering system (AJA International; Scituate, MA). Prior to the sputtering process, the electrode contact pads are coated with a layer of Shipley S1813 (MicroChem) and baked for 2 minutes at 115 °C to prevent SiO_2 deposition onto the region of IDT that requires electrical contact. The protective layer is subsequently cleaned with oxygen plasma for 5 minutes at 150 W and 40 sccm gas flow. Wafers are prepared for post processing by spinning Shipley S1813 at 3000 rpm, followed by baking at 115 °C for 2 minutes to form a protective layer. The substrate is scored with 250 μm deep lines using an automated dicing saw (DAD321, DISCO; Tokyo, Japan) and can then be broken into individual, square pieces each containing a single IDT. The protection layer and the contact pad coating are removed by soaking individual IDTs in acetone for about 15 minutes, then cleaning with isopropanol prior to use.

3.3 Soft lithography

Molds for PDMS replicas are created with multi-layer soft lithography. Layers are processed by following the method recommended in the manufacturer data sheet for SU-83000 series photoresists (MicroChem). For each layer, a small amount of resist is dispensed onto the silicon wafer, which is then spun at 3000 rpm to create a layer that is 25 μm thick. Each layer is pre-baked for a total of 12 minutes at 95 °C on the hot plate. The photomask (CAD/Art Services) for a layer is aligned to any underlying features and the layers of photoresist are patterned with UV light on a contact mask aligner (ABM; Scotts Valley, CA). The resist is then post-

exposure baked for 1 minute at 65 °C and 5 minutes at 95 °C, followed by wafer immersion in polyethylene glycol monomethyl ether acetate (484431, Sigma-Aldrich; St. Louis, MO) for 6 minutes using an orbital shaker (Roto Mix 8 × 8, Thermo Fisher; Waltham, MA) for mixing. After development, the wafer is rinsed with isopropanol and blown dry with compressed nitrogen. These steps are repeated for each layer subsequent layer. After the layers have been developed, the wafer is now ready to serve as a mold for creating PDMS replicas.

PDMS (Sylgard 184, Dow-Corning; Midland, MI) base and cross-linker in a 10∶1 weight ratio are mixed using a Thinky mixer (AR-100, Thinky; Tokyo, Japan). The PDMS is degassed for 20 minutes and the mold is cured in the oven at 65 °C overnight to create a replica. The PDMS replica is cut into individual sorting devices prior to use. Inlet and outlet holes are created with a 1.2 mm diameter biopsy punch (Uni-Core, GE Healthcare Life Sciences; Pittsburgh, PA). Individual devices are then bonded to the substrate using an oxygen plasma stripper (PE-50, Plasma Etch; Carson City, NV). During the bonding procedure, the PDMS device is aligned to the IDT so that the electrodes are situated beneath the air pocket. The PDMS device forms three sides of the device's flow channel, while the lithium niobate substrate serves as the bottom of the flow channel.

3.4 Device operation

An a RF waveform generator (SMB100A, Rhode and Schwarz; CITY) is used to create and control the power level of the RF pulse sent to the IDT, which is amplified using a high gain RF amplifier (LZY-22+, Mini-Circuits; CITY), and whose pulse length is adjusted using LabVIEW (National Instruments). For fluorescence detection, light emitted by a fluorescent bead or cell is detected by a photomultiplier tube that then generates a voltage proportional to the intensity of detected light. The voltage is then digitized by a data acquisition card (PCIe-7842R, National Instruments; CITY) and analyzed in real-time using the card's integrated field-programmable gate array (FPGA), which then triggers the RF waveform generator to send the pulse to the IDT.

4 Conclusions

Our microfluidic device uses TSAW to provide a general strategy for generating water-in-oil droplets on-demand, with controllable sizes. Our integration with standard fluorescence detection to selectively encapsulate individual particles on-demand overcomes fundamental limitations of passive devices, and may find particular use in areas where the production of empty droplets needs to be minimized or excluded, for instance where sample concentrations must remain low, or when encapsulating rare cells for single-cell sequencing. The integration of multiple capabilities on a single microfluidic device may eliminate the need for additional devices, substantially improving the efficiency and yield of the overall workflow. Furthermore, our simultaneous

lysing and encapsulation of cells could be advantageous for eliminating the use of chemical lysis agents, which may show significant differences in effects on different cell types. Finally, our TSAW-based pico-injection may afford more precise control, and unlike more traditional methods does not rely on a differences in dielectric constant, potentially improving the performance of high-throughput reactions, or in applications that require each droplet to be uniquely addressable.

Conflicts of interest

There are no conflicts to declare.

Acknowledgements

References

1 H. Song, D. L. Chen and R. F. Ismagilov, *Angew. Chem., Int. Ed.*, 2006, **45**, 7336–7356.
2 A. Theberge, F. Courtois, Y. Schaerli, M. Fischlechner, C. Abell, F. Hollfelder and W. Huck, *Angew. Chem., Int. Ed.*, 2010, **49**, 5846–5868.
3 B. Rotman, *Proc. Natl. Acad. Sci. U. S. A.*, 1961, **47**, 1981–1991.
4 T. Thorsen, R. W. Roberts, F. H. Arnold and S. R. Quake, *Phys. Rev. Lett.*, 2001, **86**, 4163–4166.
5 T. Jing, R. Ramji, M. E. Warkiani, J. Han, C. T. Lim and C.-H. Chen, *Biosens. Bioelectron.*, 2015, **66**, 19–23.
6 E. W. M. Kemna, R. M. Schoeman, F. Wolbers, I. Vermes, D. A. Weitz and A. van den Berg, *Lab Chip*, 2012, **12**, 2881–2887.
7 D. J. Collins, A. Neild, A. DeMello, A.-Q. Liu and Y. Ai, *Lab Chip*, 2015, **15**, 3439–3459.
8 L. Shang, Y. Cheng and Y. Zhao, *Chem. Rev.*, 2017, **117**, 7964–8040.
9 B. Kintses, C. Hein, M. F. Mohamed, M. Fischlechner, F. Courtois, C. Lainé and F. Hollfelder, *Chem. Biol.*, 2012, **19**, 1001–1009.
10 A. M. Klein, L. Mazutis, I. Akartuna, N. Tallapragada, A. Veres, V. Li, L. Peshkin, D. A. Weitz and M. W. Kirschner, *Cell*, 2015, **161**, 1187–1201.
11 E. Z. Macosko, A. Basu, R. Satija, J. Nemesh, K. Shekhar, M. Goldman, I. Tirosh, A. R. Bialas, N. Kamitaki, E. M. Martersteck, J. J. Trombetta, D. A. Weitz, J. R. Sanes, A. K. Shalek, A. Regev and S. A. McCarroll, *Cell*, 2015, **161**, 1202–1214.

12 S. Köster, F. E. Angilè, H. Duan, J. J. Agresti, A. Wintner, C. Schmitz, A. C. Rowat, C. A. Merten, D. Pisignano, A. D. Griffiths and D. A. Weitz, *Lab Chip*, 2008, **8**, 1110–1115.

13 J. Clausell-Tormos, D. Lieber, J.-C. Baret, A. El-Harrak, O. J. Miller, L. Frenz, J. Blouwolff, K. J. Humphry, S. Köster, H. Duan, C. Holtze, D. A. Weitz, A. D. Griffiths and C. A. Merten, *Chem. Biol.*, 2008, **15**, 427–437.

14 R. Zilionis, J. Nainys, A. Veres, V. Savova, D. Zemmour, A. M. Klein and L. Mazutis, *Nat. Protoc.*, 2017, **12**, 44–73.

15 A. R. Abate, T. Hung, P. Mary, J. J. Agresti and D. A. Weitz, *Proc. Natl. Acad. Sci. U. S. A.*, 2010, **107**, 19163–19166.

16 J.-C. Baret, O. J. Miller, V. Taly, M. Ryckelynck, A. El-Harrak, L. Frenz, C. Rick, M. L. Samuels, J. B. Hutchison, J. J. Agresti, D. R. Link, D. A. Weitz and A. D. Griffiths, *Lab Chip*, 2009, **9**, 1850–1858.

17 L. Mazutis, J. Gilbert, W. L. Ung, D. A. Weitz, A. D. Griffiths and J. A. Heyman, *Nat. Protoc.*, 2013, **8**, 870–891.

18 S.-Y. Park, T.-H. Wu, Y. Chen, M. A. Teitell and P.-Y. Chiou, *Lab Chip*, 2011, **11**, 1010–1012.

19 M. He, J. S. Kuo and D. T. Chiu, *Appl. Phys. Lett.*, 2005, **87**, 031916.

20 J. Xu and D. Attinger, *J. Micromech. Microeng.*, 2008, **18**, 065020.

21 D. J. Collins, T. Alan, K. Helmerson and A. Neild, *Lab Chip*, 2013, **13**, 3225–3231.

22 J. C. Brenker, C. Devendran, A. Neild and T. Alan, *Lab Chip*, 2020, **20**, 253–265.

23 H. Lu, K. Mutafopulos, J. A. Heyman, P. Spink, L. Shen, C. Wang, T. Franke and D. A. Weitz, *Lab Chip*, 2019, **19**, 4064–4070.

24 D. J. Collins, T. Alan and A. Neild, *Appl. Phys. Lett.*, 2014, **105**, 033509.

25 T. Franke, S. Braunmüller, L. Schmid, A. Wixforth and D. A. Weitz, *Lab Chip*, 2010, **10**, 789–794.

26 G. Destgeer, K. H. Lee, J. H. Jung, A. Alazzam and H. J. Sung, *Lab Chip*, 2013, **13**, 4210–4216.

27 D. J. Collins, A. Neild and Y. Ai, *Lab Chip*, 2016, **16**, 471–479.

28 W. L. Ung, K. Mutafopulos, P. Spink, R. W. Rambach, T. Franke and D. A. Weitz, *Lab Chip*, 2017, **17**, 4059–4069.

29 K. Mutafopulos, P. Spink, C. D. Lofstrom, P. J. Lu, H. Lu, J. C. Sharpe, T. Franke and D. A. Weitz, *Lab Chip*, 2019, **19**, 2435–2443.

30 X. Ding, J. Shi, S.-C. S. Lin, S. Yazdi, B. Kiraly and T. J. Huang, *Lab Chip*, 2012, **12**, 2491–2497.

31 M. Alghane, B. X. Chen, Y. Q. Fu, Y. Li, J. K. Luo and A. J. Walton, *J. Micromech. Microeng.*, 2010, **21**, 015005.

32 S. Shiokawa, Y. Matsui and T. Ueda, *Proc. - IEEE Ultrason. Symp.*, 1989, **1**, 643–646.

33 E. Amstad, M. Chemama, M. Eggersdorfer, L. R. Arriaga, M. P. Brenner and D. A. Weitz, *Lab Chip*, 2016, **16**, 4163–4172.

34 Z. Li, A. M. Leshansky, L. M. Pismen and P. Tabeling, *Lab Chip*, 2015, **15**, 1023–1031.

35 S. Sugiura, M. Nakajima, J. Tong, H. Nabetani and M. Seki, *J. Colloid Interface Sci.*, 2000, **227**, 95–103.

36 S. Sahin and K. Schroën, *Lab Chip*, 2015, **15**, 2486–2495.

37 A. Salehi-Reyhani, F. Gesellchen, D. Mampallil, R. Wilson, J. Reboud, O. Ces, K. R. Willison, J. M. Cooper and D. R. Klug, *Anal. Chem.*, 2015, **87**, 2161–2169.

38 E. W. Hall, S. Kim, V. Appadoo and R. N. Zare, *Micromachines*, 2013, **4**, 321–332.

39 M. Mahalanabis, H. Al-Muayad, M. D. Kulinski, D. Altman and C. M. Klapperich, *Lab Chip*, 2009, **9**, 2811–2817.

40 S. C. Kim, I. C. Clark, P. Shahi and A. R. Abate, *Anal. Chem.*, 2018, **90**, 1273–1279.

41 M. Khan, S. Mao, W. Li and J.-M. Lin, *Chem. – Eur. J.*, 2018, **24**, 15398–15420.

42 B. Bruijns, A. Van Asten, R. Tiggelaar and H. Gardeniers, *Biosensors*, 2016, **6**, 1–35.

43 S. Herminghaus, *Phys. Rev. Lett.*, 1999, **83**, 2359–2361.

44 C. Priest, S. Herminghaus and R. Seemann, *Appl. Phys. Lett.*, 2006, **89**, 134101.

45 R. Seemann, M. Brinkmann, T. Pfohl and S. Herminghaus, *Rep. Prog. Phys.*, 2011, **75**, 016601.

46 S. Jen and R. Bobkowski, An International Symposium (Cat. No.00CH37121), *Proc. - IEEE Ultrason. Symp.*, 2000, **1**, 269–273.